

# Spin-Flop Phenomenon of Two-Dimensional Frustrated Antiferromagnets without Anisotropy in Spin Space

Hiroki Nakano<sup>1 \*</sup>, Tôru Sakai<sup>1,2 †</sup>, and Yasumasa Hasegawa<sup>1 ‡</sup>

<sup>1</sup>Graduate School of Material Science, University of Hyogo, Kamigori, Hyogo 678-1297, Japan

<sup>2</sup>Japan Atomic Energy Agency, SPring-8, Sayo, Hyogo 679-5148, Japan

(Received April 4, 2024)

Motivated by a recent finding of a spin-flop phenomenon in a system without anisotropy in spin space reported in the  $S = 1/2$  Heisenberg antiferromagnet on the square-kagome lattice, we study the  $S = 1/2$  Heisenberg antiferromagnets on two other lattices composed of vertex-sharing triangles by the numerical diagonalization method. One is a novel lattice including a *shuriken* shape with four teeth; the other is the kagome lattice with  $\sqrt{3} \times \sqrt{3}$ -structure distortion, which includes a *shuriken* shape with six teeth. We find in the magnetization processes of these systems that a magnetization jump accompanied by a spin-flop phenomenon occurs at the higher-field-side edge of the magnetization plateau at one-third the height of saturation. This finding indicates that the spin-flop phenomenon found in the isotropic system on the square-kagome lattice is not an exceptional case.

## 1. Introduction

In magnetization processes of magnetic materials, each material shows various behaviors as its characteristics. One of such macroscopic behaviors is the magnetization jump. There are several microscopic origins of this jump. As a trivial case, a ferromagnetic system shows a jump in its ground-state magnetization process when the external field is changed from negative to positive values in a fixed direction. The same type of jump in magnetization occurs in a ferrimagnetic system.<sup>1</sup> There is no change in lines along microscopic spin directions between the state under a negative field and that under a positive field. As another origin of the jump, a spin-flop phenomenon<sup>2-4</sup> is widely known; the phenomenon is the occurrence of an abrupt change in lines along microscopic spin directions while the states change owing to the increase in magnetic field. We distinguish the type of magnetization jump in the ferromagnet and ferrimagnet mentioned above from the spin-flop phenomenon. It is generally understood that this phenomenon occurs when a certain anisotropy essentially exists in a magnetic system. One of the notable experimental realizations of such a spin-flop phenomenon is  $\text{CsCuCl}_3$ , whose magnetization jump is explained by the mechanism based on the spin-flop phenomenon due to the spin anisotropy of the system.<sup>5</sup>

Under these circumstances, on the other hand, a recent investigation<sup>6</sup> showed that a spin-flop phenomenon occurs in the  $S = 1/2$  Heisenberg antiferromagnet on the square-kagome (squagome) lattice shown in Fig. 1(a) despite the fact that the system has no anisotropy in spin space. This finding became a counterexample to a general understanding of the spin-flop phenomenon. Unfortunately, it is unclear whether this behavior of the model is an exceptional and rare behavior of an irregular model or a general phenomenon that is

observed in various systems sharing a spin-isotropic feature. Hereafter, the models that we consider in this study are limited to systems including Heisenberg-type interactions only.

This lattice was originally introduced in Ref. 7 from the viewpoint of the relationship between the spin model on this lattice and the eight-vertex model. A numerical study of the antiferromagnet on this lattice was also reported in Refs. 8 and 9. The lattice shares several characteristics with the kagome lattice; however, Ref. 6 showed that there is a distinct different behavior between the  $T = 0$  magnetization process of the antiferromagnet on the lattice shown in Fig. 1(a) and that of the kagome-lattice antiferromagnet at approximately the one-third height of the saturation, particularly at the higher-field edge of this height. Therefore, the finding of the spin-flop phenomenon in the Heisenberg antiferromagnet on the square-kagome lattice requires us to reexamine our understanding of the mechanism underlying the spin-flop phenomenon.

Under the above mentioned circumstances, it is important to examine whether a spin-flop phenomenon also occurs in the spin-isotropic antiferromagnet on other lattices. If it is confirmed, one finds that a spin-flop phenomenon of spin-isotropic antiferromagnets is not a rare occurrence in the square-kagome-lattice antiferromagnet. In this paper, then, let us consider the lattices shown in Figs. 1(b) and 2.

The purpose of the present study is to present the second and third examples of the spin-flop phenomenon of spin-isotropic antiferromagnets. The examples are important because they possibly lead to clarifying the mechanism of the spin-flop phenomenon and to our deeper understanding of the frustration effect in quantum systems.

The paper is organized as follows. In the next section, the model Hamiltonian and the calculation method are explained. The third section is devoted to the presentation and discussion of our main results. In the

\*E-mail: hnakano@sci.u-hyogo.ac.jp

†E-mail: sakai@spring8.or.jp

‡E-mail: hasegawa@sci.u-hyogo.ac.jp

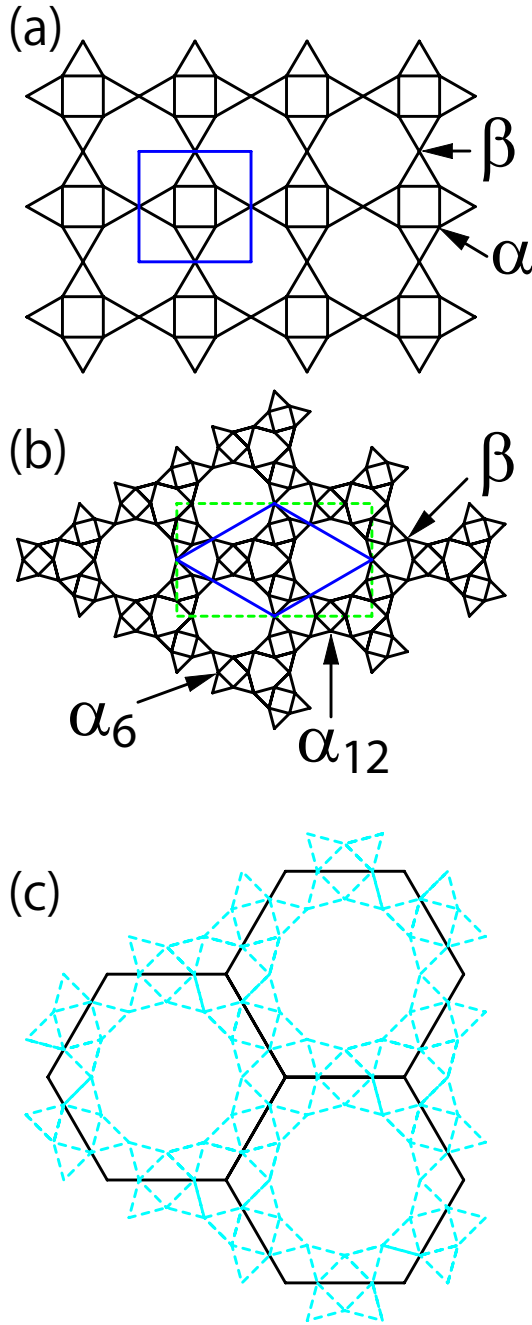


Fig. 1. (Color) (a) Square-kagome lattice and (b) *shuriken*-bonded honeycomb lattice. Blue large square in (a) and blue rhombus in (b) represent a unit cell of each lattice. In (b), a rectangle surrounded by green dotted lines denotes a finite-size cluster of  $N_s = 36$ . (c) illustrates the relationship between the ordinary honeycomb lattice (black solid line) and the *shuriken*-bonded honeycomb lattice (light blue dotted line).

final section, the conclusion and future prospects are given.

## 2. Model Hamiltonians and Method

As mentioned above, we consider the lattices illustrated in Figs. 1(b) and 2. In comparison with the situation that the square-kagome lattice shown in Fig. 1(a) includes a *shuriken* structure formed from four equivalent regular triangles in its unit cell, the lattice

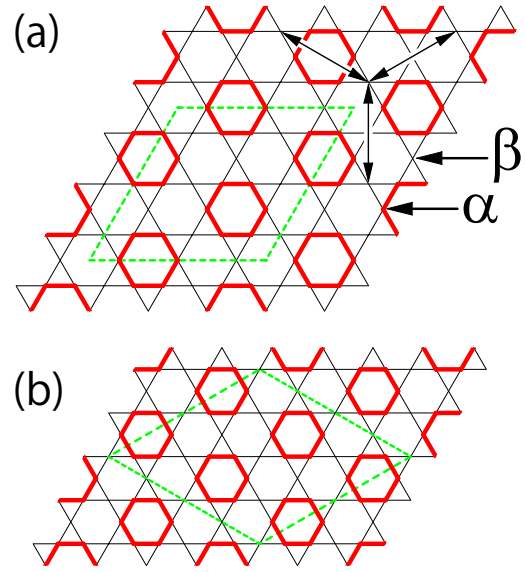


Fig. 2. (Color) The kagome lattice with distortion of  $\sqrt{3} \times \sqrt{3}$  structure is illustrated by red thick and black thin solid lines. In (a) and (b), rhombuses surrounded by green dotted lines show finite-size clusters of  $N_s = 27$  and  $36$ , respectively. An arrow with a head at each of the two edges indicates the most distant pair in the finite-size cluster in (a).

shown in Fig. 1(b) also includes the same *shuriken* structure,<sup>6</sup> but the network in the two-dimensional plane is different from that in the square-kagome lattice. As a consequence, the lattice shown in Fig. 1(b) includes three *shurikens* in its unit cell. If one replaces each *shuriken* with a simple bond, one can obtain the honeycomb lattice [see Fig. 1(c)]; therefore, let us call the lattice shown in Fig. 1(b) the *shuriken*-bonded honeycomb (SBH) lattice hereafter, because the antiferromagnet on this lattice has not been investigated to the best of our knowledge. Note here that the SBH lattice is also related to the ordinary kagome lattice because the latter is reproduced from the SBH lattice when each *shuriken* in the SBH lattice is replaced by a simple vertex at the center of the *shuriken* and when one links all the nearest-neighbor pairs of new vertices after the replacement. In the SBH lattice, there are eighteen vertices in each unit cell. Vertices are divided into three groups: one is a vertex of the square inside a *shuriken* and a vertex of the hexagon, another is a vertex of the square and a vertex of the dodecagon, and the other is a vertex of the hexagon and a vertex of the dodecagon; hereafter, let us call the vertex sites in these groups the  $\alpha_6$ ,  $\alpha_{12}$ , and  $\beta$  sites, respectively. Note here that each vertex is shared by the neighboring two triangles; thus, we have the coordination number as  $z = 4$  in the SBH lattice; the characteristics are similar to those of the ordinary kagome lattice and the square-kagome lattice.

On the other hand, the lattice in Figs. 2(a) and 2(b) is obtained by a tuning of the interaction strength at the red thick bonds in the ordinary kagome lattice. The tuning leads to the so-called  $\sqrt{3} \times \sqrt{3}$  distortion. Each unit cell includes nine vertices, six of them form a red thick hexagon. The hexagon is accompanied by six triangles in sharing their edges; the hexagon with the six

triangles seem to form another type of *shuriken* with six teeth,<sup>10</sup> in contrast to the *shuriken* with four teeth in the SBH lattice shown in Fig. 1(b). Owing to the distortion, vertices become divided into two groups: one is a vertex of a hexagon and one is not. Hereafter, let us call the vertex site in the former (latter) group the  $\alpha$  ( $\beta$ ) site. The magnetization process of the antiferromagnet on this  $\sqrt{3} \times \sqrt{3}$ -distorted kagome lattice was first described in Ref. 11, in which a similar backbending behavior in the finite-size magnetization process was observed at the higher-field edge of the one-third height of the saturation. Unfortunately, it was not able to examine whether the behavior is an artifact due the finite-size effect or a truly thermodynamic behavior within the limited system sizes treated in Ref. 11. In the present study, then, we carry out calculations of a larger cluster and obtain the magnetization process together with the information of local magnetizations, by which we tackle the backbending behavior of the antiferromagnet on the  $\sqrt{3} \times \sqrt{3}$ -distorted kagome lattice.

The Hamiltonian that we study in this research is given by  $\mathcal{H} = \mathcal{H}_0 + \mathcal{H}_{\text{Zeeman}}$ , where

$$\mathcal{H}_0 = \sum_{\langle i,j \rangle} J \mathbf{S}_i \cdot \mathbf{S}_j, \quad (1)$$

for the model on the lattice shown in Fig. 1(b) and

$$\mathcal{H}_0 = \sum_{\langle i,j \rangle \in \text{black bonds}} J_A \mathbf{S}_i \cdot \mathbf{S}_j + \sum_{\langle i,j \rangle \in \text{red bonds}} J_B \mathbf{S}_i \cdot \mathbf{S}_j, \quad (2)$$

for the model on the distorted kagome lattice shown in Fig. 2. Let us emphasize here that  $\mathcal{H}_0$  is isotropic in spin space.  $\mathcal{H}_{\text{Zeeman}}$  is given by

$$\mathcal{H}_{\text{Zeeman}} = -h \sum_j S_j^z. \quad (3)$$

Here,  $\mathbf{S}_i$  denotes the  $S = 1/2$  spin operator at site  $i$  illustrated by the vertex in Figs. 1 and 2. The sum of  $\mathcal{H}_0$  runs over all the pairs of spin sites linked by solid lines in Figs. 1 and 2. Energies are measured in units of  $J$  for the lattice shown in Fig. 1(b) and  $J_A$  for the distorted kagome lattice; hereafter, we set  $J = 1$  and  $J_A = 1$ . The number of spin sites is denoted by  $N_s$ . We impose the periodic boundary condition for clusters with site  $N_s$ , which are shown in Figs. 1(b), 2(a), and 2(b).

We calculate the lowest energy of  $\mathcal{H}_0$  in the subspace belonging to  $\sum_j S_j^z = M$  by numerical diagonalizations based on the Lanczos algorithm and/or the householder algorithm. Here,  $M$  takes an integer from zero to the saturation value  $M_s (= SN_s)$ . The energy is denoted by  $E(N_s, M)$ . To achieve calculations of large clusters, a part of Lanczos diagonalizations has been carried out using the MPI-parallelized code, which was originally developed in the study of the Haldane gaps.<sup>12</sup> The usefulness of our program was confirmed in large-scale parallelized calculations.<sup>13,14</sup>

For a finite-size system, the magnetization process is determined by the magnetization increase from  $M$  to  $M + 1$  at the field

$$h = E(N_s, M + 1) - E(N_s, M), \quad (4)$$

under the condition that the lowest-energy state with the magnetization  $M$  and that with  $M + 1$  become the ground state in specific magnetic fields. When the lowest-energy state with the magnetization  $M$  does not become the ground state in any field, the magnetization process around the magnetization  $M$  is determined by the Maxwell construction.

### 3. Results and Discussion

#### 3.1 Shuriken-bonded honeycomb lattice

First, we examine the magnetization process of the antiferromagnet on the *shuriken*-bonded honeycomb lattice shown in Fig. 1(b). Note here that the treated system sizes are  $N_s = 18$  and 36.

Figure 3 shows the results of the  $T = 0$  magnetization process. The major characteristics appear at the two-third and one-third heights of the saturation.

At the two-third height of the saturation, the magnetization plateau is accompanied by a clear jump from this height to the saturation. A similar jump is known in the ordinary kagome-lattice and square-kagome antiferromagnets. The mechanism of the jump in the kagome-lattice antiferromagnet is clarified by explicit eigenstates forming a spatially localized structure at hexagons of the kagome lattice discussed in Ref. 15. The same mechanism also holds in the square-kagome-lattice antiferromagnet; the examination was reported in Ref. 9.

At the one-third height of the saturation, a clear magnetization plateau is observed regardless of system size. An important observation is the existence of the magnetization jump at the higher edge of this height in the case of  $N_s = 36$ . The jump is not observed in the case of  $N_s = 18$  because the resolution may be low owing to the smallness of the system size.

To clarify the relationship between the magnetization jump observed in the case of  $N_s = 36$  and the spin-flop phenomenon, let us examine the local magnetization for both  $N_s = 18$  and 36. The local magnetization is evaluated as

$$m_{\text{LM}}^\xi = \frac{1}{N_\xi} \sum_{j \in \xi} \langle S_j^z \rangle, \quad (5)$$

where  $\xi$  takes  $\alpha_6$ ,  $\alpha_{12}$ , and  $\beta$ . Here, the symbol  $\langle \mathcal{O} \rangle$  denotes the expectation value of the operator  $\mathcal{O}$  with respect to the lowest-energy state within the subspace with a fixed  $M$  of interest. Note that the average<sup>16</sup> over  $\xi$  is carried out in the case of degenerated ground states for some values of  $M$ . For  $M$  with nondegenerated ground states, the results do not change regardless of the presence or absence of the average. The result is given in a plot as a function of  $M$  in Fig. 4. At least in the realized ground states, it is considered that deviations due to the difference in system size are small and that the differences between  $\alpha_6$  and  $\alpha_{12}$  are also small. One observes in the range of  $0 \leq M \leq \frac{1}{3}M_s$  that the local magnetizations at  $\alpha_6$  and  $\alpha_{12}$  sites are maintained close to zero while the local magnetization at the  $\beta$  site increases linearly with respect to  $M$ . At  $M/M_s = 1/3$ , the  $\beta$  site reveals almost a full moment in contrast to the almost vanishing moments at the  $\alpha_6$  and  $\alpha_{12}$  sites. In the range of  $\frac{1}{3}M_s + 2 < M < \frac{2}{3}M_s$ , on the other

hand, the local magnetizations at  $\alpha_6$  and  $\alpha_{12}$  sites are nonzero and close to the value of that at the  $\beta$  site. One certainly observes that an abrupt change in lines along spin directions occurs between the regions of  $M \leq \frac{1}{3}M_s$  and  $M > \frac{1}{3}M_s$ . This is indeed the spin-flop phenomenon.

Let us discuss the spin states from the above results of the local magnetizations. According to the argument of the square-kagome-lattice antiferromagnet<sup>6</sup> from the viewpoint of a classical-spin system, we focus our attention on a local triangle, in which a  $\beta$  site and an  $\alpha_6$  site, and an  $\alpha_{12}$  site are its vertices. It is clearly observed that, in the states of  $M \geq \frac{1}{3}M_s + 2$ , the local magnetizations at the  $\alpha_6$ ,  $\alpha_{12}$ , and  $\beta$  sites are nonzero but significantly smaller than the full moment. These results suggest that the spins show canting angles that are intermediate. Therefore, the states  $M \geq \frac{1}{3}M_s + 2$  suggest umbrella states. At  $M = \frac{1}{3}M_s$ , on the other hand, the result that the local moment at the  $\beta$  site shows almost a full moment indicates that the spin at the  $\beta$  site is almost parallel to the  $z$ -axis. The vanishing moments at  $\alpha_6$  and  $\alpha_{12}$  sites indicate various possibilities of spin directions of these two sites. One possibility is that the spin at the  $\alpha_6$  site and the spin at the  $\alpha_{12}$  site are almost perpendicular to the  $z$ -axis. The  $\alpha_6$  and  $\alpha_{12}$  spins should be antiparallel to each other because the total magnetization may not become polarized perpendicular to the  $z$ -axis within the consideration of a single local triangle. Although the expectation values  $\langle S_j^x \rangle$  and  $\langle S_j^y \rangle$  are zero at the  $\alpha_6$  and  $\alpha_{12}$  sites, the classical intuitive image of spin configuration at  $M = \frac{1}{3}M_s$  is the upside-down T structure,<sup>6</sup> i.e., two spins at  $\alpha_6$  and  $\alpha_{12}$  sites are antiparallel in the  $x$ - $y$  plane and three spins at  $\alpha_6$ ,  $\alpha_{12}$ , and  $\beta$  sites are in the same plane. Another possibility is that one of the  $\alpha_6$  and  $\alpha_{12}$  spins is up and that the other spin is down with respect to the  $z$ -direction. In this spin configuration, the vanishing moment is a consequence of the average of up-spins and down-spins over *shurikens*. In both cases of the configurations in the  $\alpha_6$  and  $\alpha_{12}$  spins at  $M = \frac{1}{3}M_s$ , the discontinuity from the states of  $M \geq \frac{1}{3}M_s$  can occur because there exists a significant reduction in discontinuity in  $m_{LM}^\beta$  from  $M = \frac{1}{3}M_s$  to  $M > \frac{1}{3}M_s$ . In the state at  $M = \frac{1}{3}M_s$ , if one takes the quantum nature into account, it is considered that a quantum spin singlet state, including both the configurations of the  $\alpha_6$  and  $\alpha_{12}$  spins mentioned above, is realized at a local part of two  $\alpha_6$ -site spins and two  $\alpha_{12}$ -site spins forming a square inside a *shuriken*. Although there are two singlet states in the isolated four-spin system, it is an open issue as to which of the two is the singlet in the state at  $M = \frac{1}{3}M_s$ , which should be tackled in future studies.

### 3.2 Distorted kagome lattice

Next, we examine the magnetization process of the antiferromagnet on the  $\sqrt{3} \times \sqrt{3}$ -distorted kagome lattice. We treat system sizes of  $N_s = 27$  and 36, as shown in Figs. 2(a) and 2(b), respectively. Figure 5 shows the result of the  $T = 0$  magnetization process. In the present study, let us focus our attention on the behavior around the higher-field edge of the one-third height of

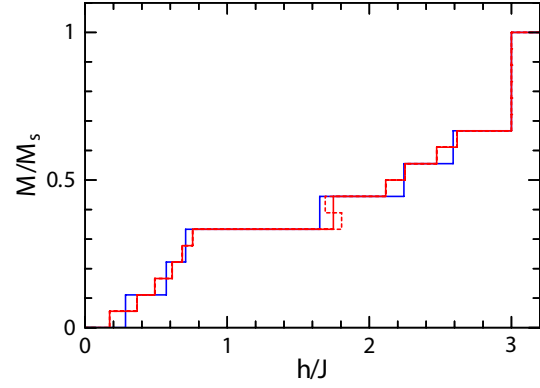


Fig. 3. (Color) Magnetization process of the antiferromagnet on the SBH lattice. The blue and red lines denote the results for  $N_s = 18$  and 36, respectively. The solid lines represent the results after the Maxwell construction while the dotted line does that before the Maxwell construction.

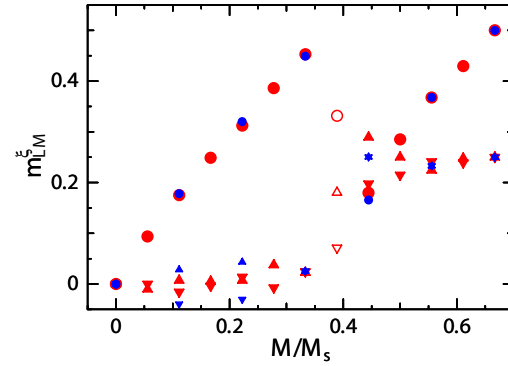


Fig. 4. (Color) Local magnetization of the state with respect to the global magnetization  $M$  in the Heisenberg antiferromagnet on the SBH lattice. Blue and red symbols denote the results for  $N_s = 18$  and 36, respectively. Circles, triangles, and reversed triangles represent the results for  $\beta$ ,  $\alpha_{12}$ , and  $\alpha_6$ , respectively. Closed symbols represent data for the stably realized states, while open symbols denote data for the unstable states at the magnetization jump.

the saturation because the brief behavior in the whole range of the magnetic field is discussed in Ref. 11.

A magnetization jump is clearly observed at the one-third height not only for  $N_s = 27$  but also for  $N_s = 36$ , although the behavior has already been detected for  $N_s = 27$ , as reported in Ref. 11. This result regardless of the system sizes suggests that the jump survives in larger systems. It is, therefore, reasonable to consider that the jump is not an artifact owing to the finite-size effect but an intrinsically thermodynamic behavior.

We examine in this subsection the behavior of  $m_{LM}^\xi$  given by Eq. (5), where  $\xi$  takes  $\alpha$  and  $\beta$ . The results are shown in Fig. 6. It is a common behavior that a local magnetization at the  $\beta$  site increases linearly to  $M = \frac{1}{3}M_s$  while that at the  $\alpha$  site is maintained at almost zero in the range of  $0 \leq M \leq \frac{1}{3}M_s$ . In the range of  $M \geq \frac{1}{3}M_s + 2$ , on the other hand, a local magnetization at the  $\alpha$  site becomes nonzero, although the values of  $m_{LM}^\xi$  are different between  $\alpha$  and  $\beta$  sites. Note here that when data of  $m_{LM}^\xi$  within the range of



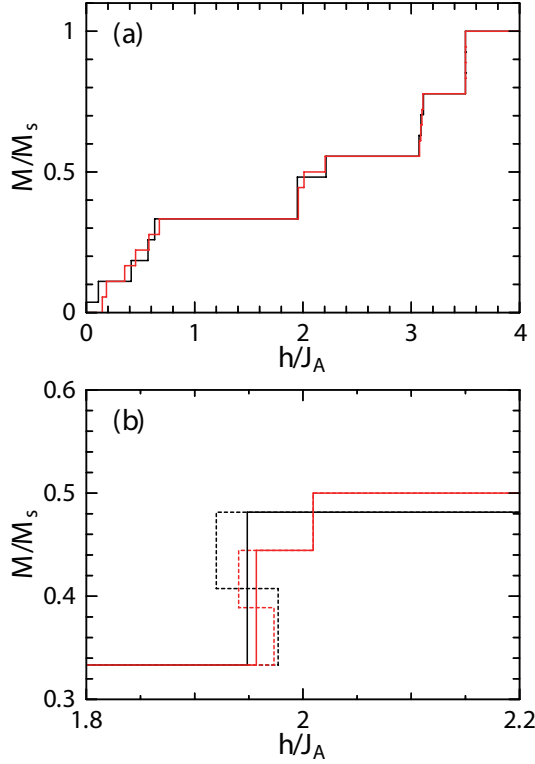


Fig. 5. (Color) Magnetization process of the antiferromagnet on the  $\sqrt{3} \times \sqrt{3}$ -distorted kagome lattice for  $J_B/J_A = 1.25$ : (a) the entire region of  $0 \leq M \leq M_s$  and (b) the zoomed-in view at around the higher-field edge of the one-third height of the saturation. Black lines and red lines denote the results for  $N_s = 27$  and  $36$ , respectively. In (b), the solid lines represent the results obtained after the Maxwell construction while the dotted lines do those obtained before the Maxwell construction.

$M \geq \frac{1}{3}M_s + 2$  are extrapolated to  $\frac{1}{3}M_s$ , extrapolated results of  $m_{LM}^\xi$  do not seem to match the corresponding values of  $m_{LM}^\xi$  at  $M = \frac{1}{3}M_s$ . This discontinuity strongly suggests an abrupt change in lines along spin directions between the regions of  $M \leq \frac{1}{3}M_s$  and  $M > \frac{1}{3}M_s$ , namely, the spin-flop phenomenon. Within the argument of classical spins of a local triangle, the situation is the same as in the case of the SBH lattice, namely, the spin state at  $M \geq \frac{1}{3}M_s + 2$  can be understood on the basis of the state of the umbrella type. In the spin state at  $M = \frac{1}{3}M_s$ ,  $\alpha$  spins form a quantum-mechanical singlet including two neighboring  $\alpha$  spins that are antiparallel to each other. Since there is a difference in the number of  $\alpha$ -site spins between the SBH lattice and the  $\sqrt{3} \times \sqrt{3}$ -distorted kagome lattice, the singlet is realized from six spins in the  $\sqrt{3} \times \sqrt{3}$ -distorted kagome lattice; the situation is more complicated. Although a difference exists, the brief behavior of spins in the case of the  $\sqrt{3} \times \sqrt{3}$ -distorted kagome lattice is common to the cases of the square-kagome lattice and the SBH lattice.

To confirm the spin direction argued above, let us consider the correlation functions  $\langle S_i^z S_j^z \rangle$  and  $\langle S_i^x S_j^x \rangle$  between a pair of sites  $i$  and  $j$ . For such examinations based on correlation functions, it is desirable to observe cases when the distance between  $i$  and  $j$  at the pair is sufficiently large and when  $i$  and  $j$  are in the same group

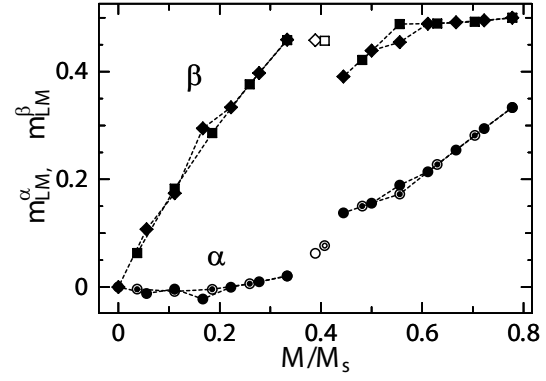


Fig. 6. Local magnetization of the state with global magnetization  $M$  in the Heisenberg antiferromagnet on the  $\sqrt{3} \times \sqrt{3}$ -distorted kagome lattice for  $J_B/J_A = 1.25$ .  $m_{LM}^\alpha$  for  $N_s = 27$  and  $N_s = 36$  are shown by circles and double circles, respectively.  $m_{LM}^\beta$  for  $N_s = 27$  and  $N_s = 36$  are shown by diamonds and squares, respectively. Closed symbols represent data for the stably realized states while open symbols denote data for the unstable states at the magnetization jump.

Table I. Correlation functions for  $N_s = 27$  cluster at  $J_B/J_A = 1.25$ . We select a pair of sites  $i$  and  $j$  so that the distance between these sites is the largest in this cluster.

		$M = \frac{1}{3}M_s$	$M = \frac{1}{3}M_s + 2$
$i, j \in \alpha$	$\langle S_i^z S_j^z \rangle$	0.00016	0.02548
	$\langle S_i^x S_j^x \rangle$	0.00099	0.00642
$i, j \in \beta$	$\langle S_i^z S_j^z \rangle$	0.21024	0.17637
	$\langle S_i^x S_j^x \rangle$	-0.00157	0.01497

of sites, namely,  $\alpha$  or  $\beta$ . It is difficult in such studies as the present one based on numerical-diagonalization calculations to realize a situation that these conditions are satisfied completely. Even in this situation, it is helpful to observe data of correlation functions  $\langle S_i^z S_j^z \rangle$  and  $\langle S_i^x S_j^x \rangle$  when  $i$  and  $j$  in the same group are the most distant in finite-size clusters. The  $N_s = 27$  cluster is this case in the present study.<sup>17</sup> The most distant pair in the  $N_s = 27$  cluster is illustrated in Fig. 2(a). Table I shows results for the two cases of  $M$  around the magnetization jump. At  $M = \frac{1}{3}M_s$ , only  $\langle S_i^z S_j^z \rangle$  for  $i, j \in \beta$  is dominant, and the absolute values of other quantities are very small. These results agree well with the result of local magnetizations, where  $m_{LM}^\beta$  is almost saturated and  $m_{LM}^\alpha$  is almost vanishing at  $M = \frac{1}{3}M_s$ . At  $M = \frac{1}{3}M_s + 2$ , on the other hand,  $\langle S_i^z S_j^z \rangle$  for  $i, j \in \beta$  becomes slightly smaller than that at  $M = \frac{1}{3}M_s$ ;  $\langle S_i^x S_j^x \rangle$  for  $i, j \in \beta$  increases from that at  $M = \frac{1}{3}M_s$ . These results indicate that a  $\beta$ -site spin leans from the  $z$ -axis. For  $i, j \in \alpha$ , both  $\langle S_i^z S_j^z \rangle$  and  $\langle S_i^x S_j^x \rangle$  at  $M = \frac{1}{3}M_s + 2$  become larger than those at  $M = \frac{1}{3}M_s$ . These results suggest that an  $\alpha$ -site spin also leans from the  $z$ -axis. These leans of  $\alpha$ - and  $\beta$ -site spins are consistent with the state of the umbrella-type suggested from the discussion based on the local magnetizations. Note that these results for the single  $N_s$  should be reexamined in future studies from the viewpoint of system-size dependences.

Finally, let us investigate the region of an interaction

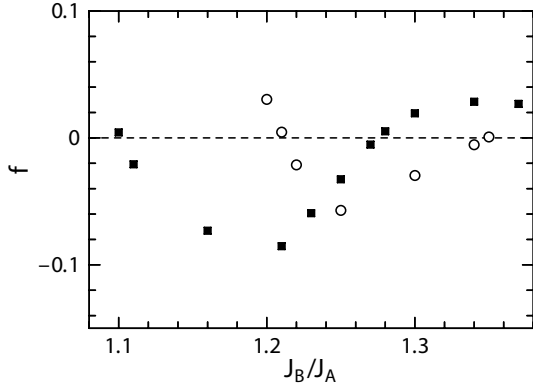


Fig. 7.  $J_B$  dependence of  $f$  at the one-third height of the saturation in the magnetization process. Open circles and closed squares denote the result of  $f$  for  $N_s = 27$  and  $N_s = 36$ , respectively.

parameter where the magnetization jump appears in the magnetization process of the antiferromagnet on the  $\sqrt{3} \times \sqrt{3}$ -distorted kagome lattice. Recall here that it has already been pointed out that the region is narrow for  $N_s = 27$  in Ref. 11. To clarify the region, we evaluate

$$f = E(N_s, M) - 2E(N_s, M + 1) + E(N_s, M + 2), \quad (6)$$

at  $M = (1/3)M_s$ . If the quantity  $f$  is negative, the backbending behavior is realized before the Maxwell construction is carried out. The result is shown in Fig. 7. The region is  $1.21 \lesssim J_B/J_A \lesssim 1.35$  and  $1.10 \lesssim J_B/J_A \lesssim 1.28$  for  $N_s = 27$  and 36, respectively. The widths of the two regions are almost the same; it becomes larger when the system sizes are increased. This behavior of the width suggests that the region survives in the thermodynamic limit. Another interesting feature is that the region of  $N_s = 36$  is closer to the undistorted kagome point of  $J_A = J_B$  than that of  $N_s = 27$ . At the present stage, it is difficult to examine what the difference in the position of the region means because the height of the unstable state of  $M = \frac{1}{3}M_s + 1$  is different between  $N_s = 27$  and 36. Recall that just at  $J_A = J_B$ , the behavior at the higher-field edge of the one-third height of the saturation in the magnetization process is continuous between  $M = \frac{1}{3}M_s$  and  $M > \frac{1}{3}M_s$  as a characteristic of the magnetization ramp<sup>18–21</sup> proposed in the kagome-lattice antiferromagnet: the continuity is observed not only in the magnetization but also in its gradient. It is worth emphasizing that the region at  $J_B/J_A \sim 1.2$  where the magnetization jump appears owing to the spin-flop phenomenon is located very close to the undistorted point  $J_B = J_A$  at which the continuous behavior is realized. The relationship between the two cases will be clarified in future studies. Near the undistorted point  $J_B = J_A$ , another ferromagnetic phase of the non-Lieb-Mattis type is known to be realized<sup>22,23</sup> owing to a distortion of a different type. Further investigations from various viewpoints are required to understand much better the physics of the undistorted point  $J_B = J_A$ .

#### 4. Conclusion and Remarks

We have studied the Heisenberg antiferromagnet on the two types of two-dimensional lattices, the kagome lattice with distortion and the *shuriken*-bonded honeycomb lattice, by the numerical diagonalization method. The magnetization processes of these models have been investigated. Our particular interest is the behavior at the one-third height of the saturation, where we detect the magnetization jump at the higher-field edge at the height. We successfully confirm that the jump occurs as a consequence of the spin-flop phenomenon from the analysis of local magnetizations and correlation functions.<sup>24</sup> The present result indicates that such a spin-flop phenomenon is not just a rare incident in the square-kagome-lattice antiferromagnet but occurs in other various cases despite the fact that all these systems are isotropic in spin space. The present result also clarifies that not only the *shuriken* structure with four teeth is a trigger but a different *shuriken* structure with six teeth also induces the spin-flop phenomenon. In the magnetization process of the Heisenberg antiferromagnet on the Cairo pentagon lattice,<sup>25,26</sup> a similar behavior of magnetization jump appears. Since this lattice does not include the structure of triangles in it, it is an interesting example, and the results will be reported in separate papers.<sup>27,28</sup>

Jumps in the magnetization process are observed in several cases within the isotropic quantum Heisenberg antiferromagnets. One is the one-dimensional case in Ref. 29. The origin of the jump is also magnetic frustration; however, it is presently unclear whether a spin-flop phenomenon occurs because the local moment and other microscopic information about the spin state have not been investigated. Other cases of the magnetization jump are two finite-size systems of the Heisenberg clusters on an icosahedron<sup>30</sup> and a dodecahedron.<sup>31</sup> However, one cannot increase the number of spins systematically to that of an infinite system within the condition that one considers regular polyhedra. In this sense, it is difficult to compare the results of the present cases and the finite-size clusters on polyhedra. The jump of the icosahedron system appears only for a large spin amplitude of  $S = 4$ , whereas no jump is observed in the case of  $S < 4$ . Investigations of the present antiferromagnets of larger- $S$  spins might be helpful for capturing the relationship between these cases. It is also known that magnetization jumps appear below  $M/M_s \leq 1/2$  in the magnetization process of the Shastry-Sutherland model in a strongly dimerized case.<sup>32</sup> Magnetization jumps can also appear when other spin-isotropic interactions are added to the isotropic quantum Heisenberg antiferromagnets. In Refs 33 and 34, the jumps and the spin structure when the multiple-spin exchange interactions exist in addition to the Heisenberg triangular-lattice model are reported. Reference 35 clarified the appearance of the jump in the bilinear-biquadratic model on the pyrochlore lattice when the biquadratic terms are switched on. Thus, one finds that there are various origins of the magnetization jumps even though the system is isotropic in spin space.

It has been clarified that magnetization jumps due to the spin-flop phenomenon occur more generally in frustrated quantum spin systems without anisotropy in spin space than we thought, even in fundamental cases composed of only Heisenberg interactions. The present models are typical ones among them. The present results strongly suggest a reconsideration of the mechanism underlying the spin-flop phenomenon. Further investigations of the spin-flop phenomenon and the magnetization jump would contribute much to our understanding of the frustration effect in magnetic materials.

### Acknowledgments

We wish to thank Professors K. Hida, M. Isoda, Y. Hosokoshi, T. Ono, and Dr. N. Todoroki for fruitful discussions. This work was partly supported by Grants-in-Aid (Nos. 23340109, 23540388, and 24540348) from the Ministry of Education, Culture, Sports, Science and Technology (MEXT) of Japan. Nonhybrid thread-parallel calculations in numerical diagonalizations were based on TITPACK version 2 coded by H. Nishimori. Some of the computations were performed using facilities of the Department of Simulation Science, National Institute for Fusion Science; Center for Computational Materials Science, Institute for Materials Research, Tohoku University; Supercomputer Center, Institute for Solid State Physics, The University of Tokyo; and Supercomputing Division, Information Technology Center, The University of Tokyo. This work was partly supported by the Strategic Programs for Innovative Research, MEXT, and the Computational Materials Science Initiative, Japan. The authors would like to express their sincere thanks to the staff of the Center for Computational Materials Science of the Institute for Materials Research, Tohoku University, for their continuous support of the SR16000 supercomputing facilities.

- 1) T. Sakai and K. Okamoto, Phys. Rev. B **65**, 214403 (2002).
- 2) L. Néel, Ann. Phys. Paris **5**, 232 (1936).
- 3) M. Kohno and M. Takahashi, Phys. Rev. B **56**, 3212 (1997).
- 4) T. Sakai and M. Takahashi, Phys. Rev. B **60**, 7295 (1999).
- 5) T. Nikuni and H. Shiba, J. Phys. Soc. Jpn. **64**, 3268 (1994).
- 6) H. Nakano and T. Sakai, J. Phys. Soc. Jpn. **82**, 083709 (2013).
- 7) R. Siddharthan and A. Georges, Phys. Rev. B **65** (2001) 014417.
- 8) P. Tomczak and J. Richter, J. Phys. A: Math. Gen. **36**, 5399 (2003).
- 9) J. Richter, J. Schulenburg, P. Tomczak, and D. Schmalfß, Condens. Matter Phys. **12**, 507 (2009).
- 10) A *shuriken* is a palm-sized weapon used by a *ninja*. Several types of *shurikens* exist; there are various numbers of teeth of a *shuriken* although the four-tooth type is well known.
- 11) K. Hida, J. Phys. Soc. Jpn. **70**, 3673 (2001).
- 12) H. Nakano and A. Terai, J. Phys. Soc. Jpn. **78**, 014003 (2009).
- 13) H. Nakano and T. Sakai, J. Phys. Soc. Jpn. **80**, 053704 (2011).
- 14) H. Nakano and T. Sakai, J. Phys. Soc. Jpn. **82**, 043715 (2013).
- 15) M. E. Zhitomirsky and H. Tsunetsugu, Phys. Rev. B **70**, 100403 (2004).
- 16) Averaging was also carried out to obtain the data shown in Fig. 6 of Ref. 6, although the authors forgot to mention it in their paper.
- 17) Note, on the other hand, that the site groups of  $i$  and  $j$  for the most distant pair in the  $N_s = 36$  cluster are different from each other.
- 18) H. Nakano and T. Sakai, J. Phys. Soc. Jpn. **79**, 053707 (2010).
- 19) T. Sakai and H. Nakano, Phys. Rev. B **83**, 100405(R) (2011).
- 20) H. Nakano and T. Sakai, Phys. Status Solidi B **250**, 579 (2013).
- 21) H. Nakano and T. Sakai, to be published in JPS Conference Proceedings.
- 22) H. Nakano, T. Shimokawa, and T. Sakai, J. Phys. Soc. Jpn. **80**, 033709 (2011).
- 23) T. Shimokawa and H. Nakano, J. Phys. Soc. Jpn. **81**, 084710 (2012).
- 24) Analysis of correlation functions for the case of the SBH lattice has not been carried out in the present study because the analysis becomes more complicated owing to the fact that the SBH lattice includes more spin sites in its unit cell. The analysis will be performed in future studies.
- 25) E. Ressouche, V. Simonet, B. Canals, M. Gospodinov, and V. Skumryev, Phys. Rev. Lett. **103**, 267204 (2009).
- 26) I. Rousochatzakis, A. M. Läuchli, and R. Moessner, Phys. Rev. B **85**, 104415 (2012).
- 27) H. Nakano, M. Isoda, and T. Sakai, J. Phys. Soc. Jpn. **83**, 053702 (2014).
- 28) M. Isoda, H. Nakano, and T. Sakai, to be published in J. Phys. Soc. Jpn.
- 29) A. Honecker, F. Mila, and M. Troyer, Eur. Phys. J. B **15**, 227 (2000).
- 30) C. Schröder, H. J. Schmidt, J. Schnack, and M. Luban, Phys. Rev. Lett. **94**, 207203 (2005).
- 31) N. P. Konstantinidis, Phys. Rev. B **72**, 064453 (2005).
- 32) T. Momoi and K. Totsuka, Phys. Rev. B **62**, 15067 (2000).
- 33) K. Kubo and T. Momoi, Z. Phys. **103**, 485 (1997).
- 34) T. Momoi, H. Sakamoto, and K. Kubo, Phys. Rev. B **59**, 9491 (1999).
- 35) K. Penc, N. Shannon, and H. Shiba, Phys. Rev. Lett. **93**, 197203 (2004).